Nanoindentation study of a Cu/Ta/SiO_2/Si multilayer system*

Zhang Xin(张昕)[1], Lu Qian(卢茜)[1], Wu Zijing(吴子景)[1], Wu Xiaojing(吴晓京)[1, 2, †], Shen Weidian[3], and Jiang Bin(蒋宾)[4]

[1]Department of Materials Science, Fudan University, Shanghai 200433, China
[2]Micro-Nanoelectronics Platform, Fudan University, Shanghai 200433, China
[3]Department of Physics and Astronomy, Eastern Michigan University, Ypsilanti, MI 48197, USA
[4]Shanghai Integrated Circuit R&D Center, Shanghai 201203, China

Abstract: Tantalum and copper layers were deposited on a thermally oxidized Si substrate in a magnetron sputtering process. Nanoindentation was adopted to investigate the hardness and elastic modulus of the Cu/Ta/SiO_2/Si multilayer system. The hardness shows an apparent dependence on the film thickness, and decreases with the increase of film thickness, whereas the elastic modulus does not. To reveal the structural change, a trench through the center of a residual indent was cut by a focused ion beam, and then examined using an ion-microscope. TEM analysis showed that delamination occurs at the interface between the Ta and the SiO_2 layer of the residual indent, suggesting that the destruction under a relatively large load is due to weak bonding.

Key words: copper; tantalum; nanoindentation; hardness; elastic modulus
DOI: 10.1088/1674-4926/33/4/043002 **EEACC:** 2520

1. Introduction

With the increase of circuit density and the downsizing of feature sizes to the nanoscale, resistance capacitance (RC) delay introduced by interconnection metallization has become a decisive factor for the performance of integrated circuits (IC). As early as in the 1990s, the feasibility of using copper for the metallization of ultra-large-scale integrated circuits (ULSI) has been evaluated[1, 2], and its first application was carried out in 0.25 μm products[3]. Nowadays, copper ($\rho = 1.7$ $\mu\Omega$·cm) has been widely adopted as a substitute for aluminum ($\rho = 2.7$ $\mu\Omega$·cm) as the interconnection metallization in ULSI processes with nodes of 90 nm and below[4−7].

However, suitable etchants for copper patterning were not yet available[8]. Damascene and dual-damascene were then introduced as the standard methods for copper interconnect patterning[9, 10]. To prevent the diffusion of Cu, it is crucial to deposit a barrier layer (such as a tantalum layer) between Cu and the dielectrics[7, 11]. The Cu liner is formed by electrochemical deposition (ECD) and planarized by chemical mechanical polishing (CMP)[12−14].

It is confirmed that the hardness and the film-thickness-dependent elastic modulus significantly influence the electromigration and stress-induced migration failures of ICs[15]. Failure mechanisms, electrical and thermal properties of the up-to-date Cu/Ta/SiO_2/Si structure have been already studied[16−18]. Moreover, CMP damage was mentioned as a primary challenge for the manufacture of interconnect structures both below and over the feature size of 32 nm[19]. However, no specific report on the mechanical and nano-tribological properties of such structures has been reported yet.

Nanoindentation is a widely applied method to measure the mechanical properties of both bulk and thin-film materials from micron to nanometer scale[20−32]. Previous research has mainly focused on copper thin films deposited directly on silicon or oxidized silicon substrate, and all of the studied samples were much thicker than the actual thickness of the copper film used in IC devices[24−27]. Furthermore, it seems more important to regard the Cu/Ta/SiO_2/Si structured film as a whole when characterizing the nanoindentation behavior.

In this paper, a series of Cu/Ta/SiO_2/Si samples were studied by using the nanoindentation method. The hardness and elastic modulus of the samples were determined by using the Oliver and Pharr method[21]. The relationship between the mechanical properties and the copper layer thickness was discussed, and the microstructure at the residual indent was studied in detail using a scanning electron microscope (SEM), a scanning ion microscope (SIM), as well as a transmission electron microscope (TEM).

2. Experimental

2.1. Sample preparation

Before the deposition of the Cu and Ta films, 270-nm-thick SiO_2 layers were first grown on the Si (111) substrates by thermal oxidation. All Cu and Ta layers were deposited by magnetron sputtering (Discovery 18, Denton Vacuum Inc.) working at a pressure of 2.6×10^{-6} Torr and a radio frequency power of 500 W. The details of the deposition parameters are listed in Table 1. A 50-nm-thick Ta buffer layer was first deposited on each oxidized substrate. Cu layers with thicknesses of 100–500 nm at 100 nm intervals were precipitated after the deposition of Ta, and labeled correspondingly as C1–C5. A

* Project supported by the Science and Technology Commission of Shanghai Municipality, China (No. 0552nm049) and the Shanghai Leading Academic Discipline Project, China (No. B113).
† Corresponding author. Email: wuxj@fudan.edu.cn
Received 23 September 2011, revised manuscript received 19 October 2011
© 2012 Chinese Institute of Electronics

Table 1. Deposition parameters for the Cu and Ta layers.

Parameter	Cu	Ta
Target diameter (mm)	76.2	76.2
Target purity (%)	99.99	99.9
Voltage (V)	430	370
DC current (A)	0.5	0.27
Deposition rate (nm/min)	30	13.3
Layer thickness (nm)	100–500	50

sample without a Cu top layer (labeled as C0) was prepared as a reference.

2.2. Nanoindentation tests

Nanoindentation tests were conducted on the $Cu/Ta/SiO_2/Si$ thin films mentioned above using an MTS Nano Indenter XP nanohardness tester. The indenter tip was a Berkovich tip with a tip radius of 200 nm and a tip angle of 120°. The multiple-loading method was adopted to measure the hardness and elastic modulus. Each sample was indented at nine different sites in a three-by-three matrix with a spacing of 100 μm. Each site was indented multiple times with an increasing maximum load starting from 0.25 mN up to 32 mN, doubling the load each time. The loading time was set to 30 s, and the holding time at maximum load was set to 30 s to minimize the creep effect. The unloading time to 90% of the maximum value was also set to 30 s. Three such periods formed a loading/unloading cycle.

Hardness and elastic modulus were calculated by using the Oliver and Pharr method[21, 30]. The contact area of the indent can be estimated as a function of contact depth, and hence hardness can be calculated by $H = P_{\max}/A_c$, where $P_{\max}$ stands for the maximum load applied and A_c for the residual contact area.

The derivative dP/dh at the point of maximum load is termed as contact stiffness S, and can be calculated by:

$$S = \frac{dP}{dh} = \frac{2}{\sqrt{\pi}} E_r \sqrt{A}, \tag{1}$$

where A is the projected contact area, and h is the hardness. Then the reduced modulus E_r can be calculated. The elastic modulus of the sample is derived from:

$$\frac{1}{E_r} = \frac{1-\nu^2}{E} + \frac{1-\nu_i^2}{E_i}, \tag{2}$$

where E and ν are the elastic modulus and Poisson's ratio of the sample, E_i and ν_i are the Elastic modulus and Poisson's ratio of the indenter tip ($\nu_i = 0.07$ for a diamond tip[20]).

2.3. Cross-sectional observation of residual indent

Cross-sectional analysis was performed on an FEI Quanta 200 3D dual beam environmental scanning electron microscope (ESEM). The electron gun and the ion gun were placed at an angle of 52°, as shown Fig. 1(a). The incidence angle of the ion beam to the surface is 90°. Before the FIB process, a thin Au layer (~5 nm) was deposited to enhance conductivity. One of the nine indents on sample C4 was bombarded by a Ga ion beam to create a trench through the center of the residual indent. Another trench was etched on sample C4 where no indent existed for reference. The depths of the trenches reduce linearly from the center to the rim of the indents to form a cross-section in the shape of an isosceles triangle. After the trench etching, the morphology studies of the vertical cross-section of the residual indent were taken using an SEM and an SIM. The tilting angles of the sample to the electron and ion beam were set to 45° to ensure that the incident beam was parallel to the hypotenuse of the isosceles-triangle-shaped trench, as illustrated in Fig. 1(b). A TEM cross-sectional sample was then prepared for the FIB process after the deposition of a Pt layer to protect the top layers. EDX spectra of three different areas in the residual indent were also taken.

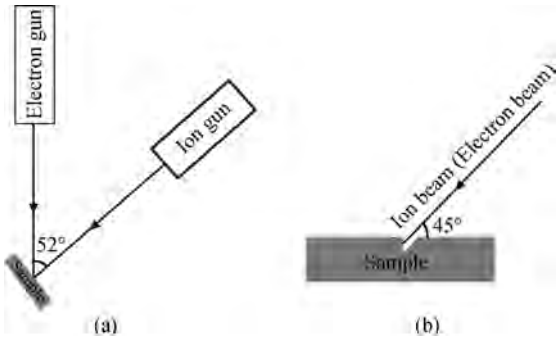

Fig. 1. Schematics of (a) the dual beam ESEM and (b) beam-sample incidence angle.

3. Results and discussion

3.1. Topography

Figure 2(a) shows the cross sectional SEM morphology of the $Ta/SiO_2/Si$ thin film. The thicknesses of the SiO_2 layer (277 nm) and Ta layer (49 nm) were controlled quite well. Figure 2(b) shows the SEM image of sample C4, which has a 400 nm-thick copper layer on top. The total thickness of the Cu and Ta layers is a little over 450 nm, but still controlled fairly well. Figure 3 (a) shows the matrix of the indents on sample C4, and a single indent showing "pile-up" is shown in Fig. 3(b). In the morphology of the residual indent, the side length of the equilateral triangle in red is 3.80 μm. The depth of the residual indent is supposed to be 0.87 μm by calculation. It is clear in Fig. 3(a) that the largest indentation depth on sample C4 is about 1.05 μm. Therefore, the relatively small residual indent depth obviously indicates an elastic recovery, and will be discussed later.

3.2. Hardness and elastic modulus

As indicated in Fig. 4, under very small indentation depths (shorter than 50 nm), the hardness of sample C0 increases from 10 to about 11 GPa with the increase of indentation depth. The increase in hardness slows down when the indentation depth is over 50 nm, and reaches 13 GPa under an indentation depth of about 260 nm. In this case, the hardness value of β-Ta is double that of SiO_2, and the $Ta/SiO_2/Si$ structure has a rather small thickness of Ta layer. Since the hardness obtained under the displacements between 50 and 260 nm is an intermediate value between that of β-Ta and SiO_2, the hardness can be attributed

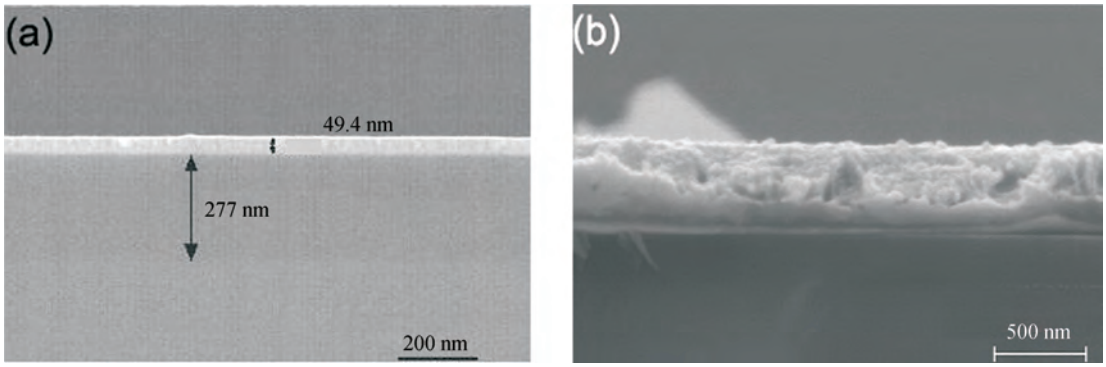

Fig. 2. Cross-sectional SEM image of samples (a) C0 and (b) C4.

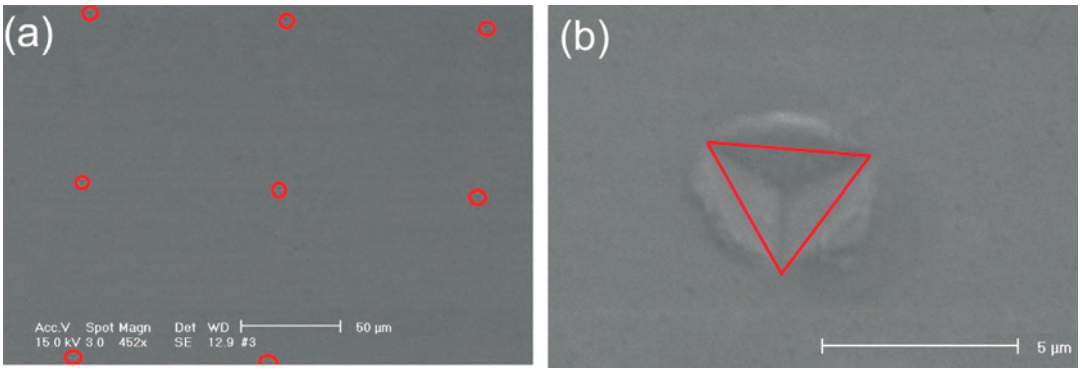

Fig. 3. SEM images of (a) the matrix of indents (surrounded by circles) on sample C4 and (b) an indent on C4 showing "pile-up" around the indented area.

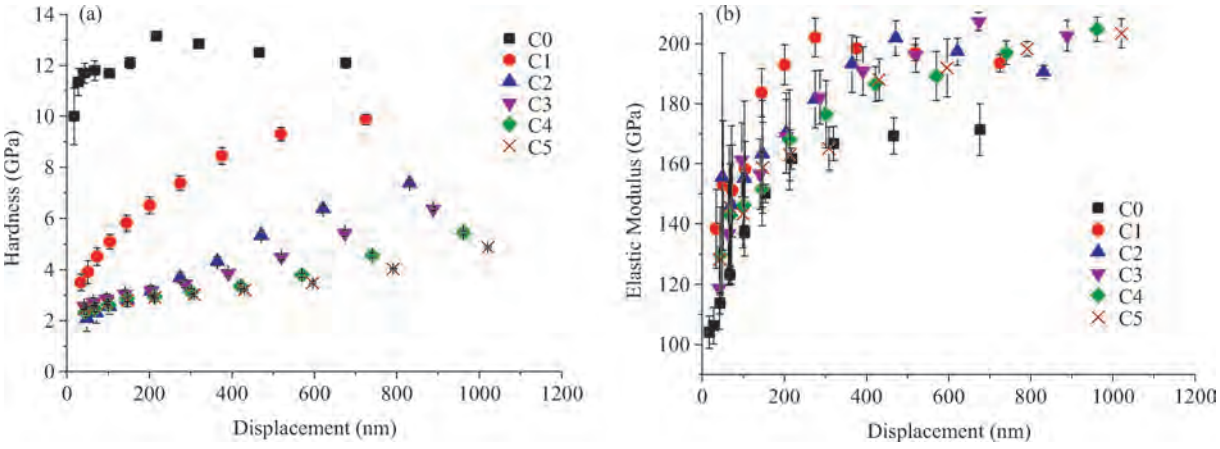

Fig. 4. (a) Hardness versus indentation depth and (b) elastic modulus versus indentation depth for the multilayer samples.

to the contribution of SiO_2. When the indentation depth reaches 260 nm and further goes beyond 320 nm (where the interface of SiO_2 and Si is supposed to be), the hardness remains almost the same, with only slight decrease. The hardness between 12 and 13 GPa is very close to the typical value of a Si monocrystal. However, the slight decrease in hardness may indicate fractures or cracks in the Si substrate, as can be observed also in sample C4, which will discussed later.

The hardness values of samples C1–C5 under each lowest load are all very close to 3 GPa, which is almost the same as in previous studies[24, 25] concerning the hardness of Cu thin films measured by nanoindentation. However, the hardness of thinner films (C1, C2 and C3) apparently increases when the indent becomes deeper, whereas the hardness of thicker films (C4 and C5) remains low and experiences less increase as the indent becomes deeper.

Besides the indent area, the contiguous plastic deformation zone also expands both in volume and depth. So there could be plastic-deformation-induced fractures or cracks before the tip reaches the SiO_2 layer and Si substrate. If there are pre-existing fractures or cracks, a considerable proportion of power that the indent tip exerts is supposed to be absorbed by the underlying SiO_2 layer and Si substrate, thus only leading to a moderate increase in composite hardness for samples C1, C2 and

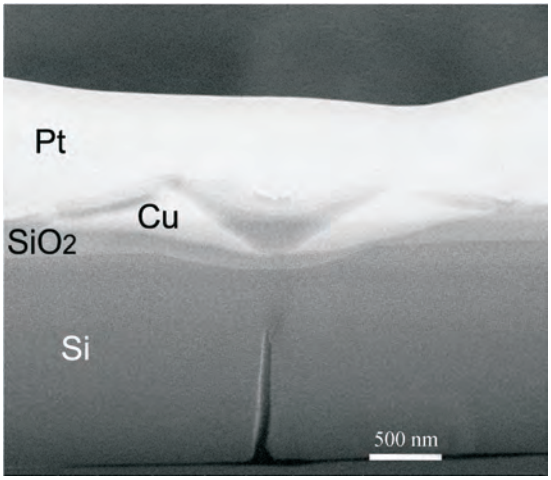

Fig. 5. SEM image showing an apparent fracture in Si substrate of cross-sectional sample prepared by FIB from sample C4.

C3. However, for sample C0 (without copper layer), the possible pre-existing fractures or cracks in the SiO_2 layer and the Si substrate may be responsible for the decrease of composite hardness when the indentation depth exceeds 150 nm.

In the case of samples C4 and C5, the composite hardness does not greatly increase with the indentation depth. Because of the thicker Cu top layers, the increase in thickness may offset the increase in hardness while the indenter tip penetrates through the Cu and Ta layers into SiO_2. The creep of Cu and Ta could absorb a considerable portion of energy exerted by the indenter tip, resulting in very small change in composite hardness throughout all indentation depths. Moreover, even before the indenter tip pierced the SiO_2 layer and the Si substrate, the load already became large enough to create cracks or fractures in the SiO_2 and the Si substrate, as in the example shown in Fig. 5. When the penetration deepened with the increase in the applied load, the cracks or fractures propagated to release the energy exerted by the indenter tip. Therefore, no great increase in composite hardness could be observed.

From Fig. 4, the elastic modulus of all samples increases with the indentation depth to a constant high value regardless of the thickness of the Cu top layer. Such a phenomenon suggests that the stiff substrate gradually predominates in the comprehensive properties of the thin film system, and the higher elastic modulus indicates a natural tendency to crack or fracture rather than ductile deformation. The elastic modulus data also supported the conclusion drawn in the discussion of Fig. 4, i.e., the SiO_2 layer and the Si substrate deform before indenter tip penetrates the metal layers as the stress field reaches the layer below.

According to a previous study[15], the elastic modulus of Cu thin film with a thickness over 80 nm is supposed to be the theoretical value (about 130 GPa), and tends to decrease when the thickness is below 80 nm. The elastic modulus values of our samples match the literature data as collected in Table 2, especially C1, C2 and C3, when the indenter tip does not penetrate through the copper layer. With regard to the elastic modulus, the underlying Ta layer does not have an apparent influence on the top Cu layer due to the relatively small thickness. For the modulus values of samples C1, C2, and C3 with relatively

Table 2. Literature data of hardness and elastic modulus for reference.

Sample	Hardness (GPa)	Elastic modulus (GPa)
Cu	~ 3[24, 25]	~ 128[28]
β-Ta	~ 16[29]	~ 195[28]
SiO_2	~ 8[23]	~ 75[23]
Si	~ 13[22]	~ 136[22]

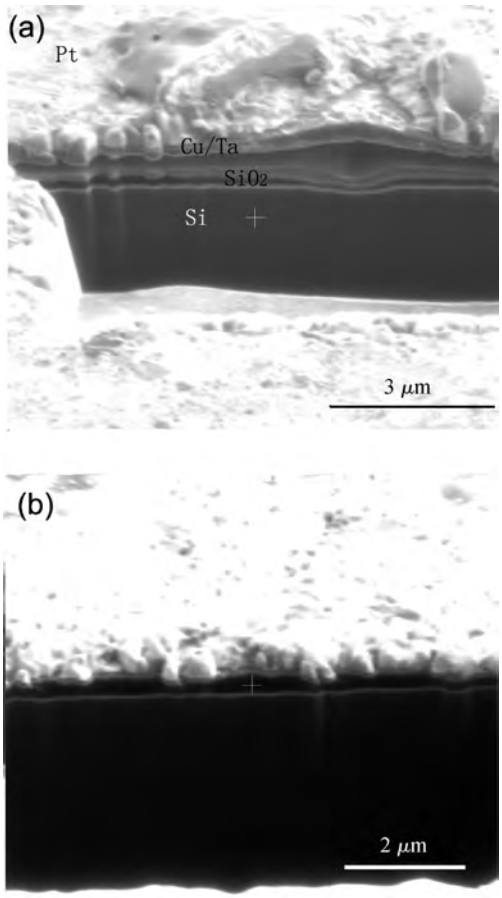

Fig. 6. SIM images of the cross section (a) through the center of a residual indent and (b) where was no indented on sample C4.

larger displacement, as suggested above, the plasticity of SiO_2 and Si (which also have the possibility of crack and fracture within) could contribute to the decrease in elastic modulus.

3.3. Delamination at Ta/SiO_2 interface

To investigate the possible existing crack in the SiO_2 layer or the Si substrate, FIB was employed to conduct cross-sectional observation of the residual indent on sample C4. The following SIM observation confirmed the existence of delamination, as presented in Fig. 6(a). The top layer is convex, while the underlying layers and the substrate are concave. Figure 6(b) provides a typical SIM image of cross-sectional sample without a nearby indent, and the layers adhere to each other very well.

A TEM cross-sectional sample was then fabricated in situ by FIB to clarify the details of delamination. Although a Pt layer was deposited on the sample surface, the top Cu and Ta layers at the center of the residual indent were de-

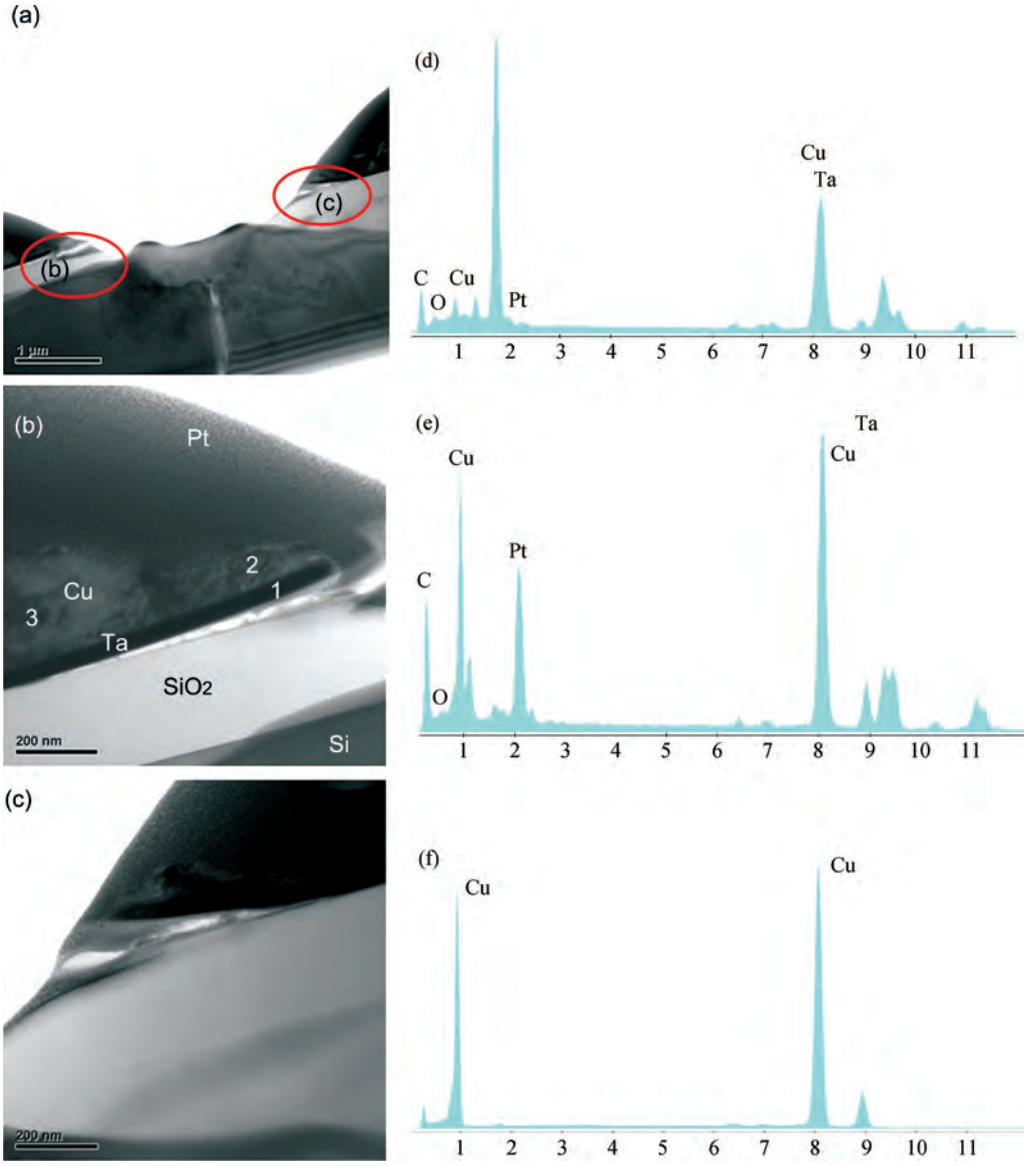

Fig. 7. (a) TEM cross-sectional image of the residual indent. (b), (c) Zoom in of the circles in (a) showing the delamination at Ta/SiO_2 interface. (d), (e), (f) EDX spectra obtained from locations 1, 2 and 3 in (b).

stroyed following the FIB process. However, from the TEM images in Fig. 7, the delamination can still be observed clearly. EDX spectra taken at three different positions, as illustrated in Fig. 7(b), are shown in Figs. 7(d), 7(e) and 7(f), indicating that the delamination occurs at the Ta/SiO_2 interface.

The fracture shown in Fig. 5 (in Si substrate just beneath the center of the residual indent) cannot be observed in Fig. 7(a). This is because the accumulated residual strain in the Si substrate was released in a bursting way when the constraint from the adjacent part was removed by the FIB process. From the TEM images, it can be deduced that the stress spreading in the Si substrate already became large enough to cause a fracture, even though the SiO_2 layer was not penetrated.

The reason why the delamination occurred at the Ta/SiO_2 interface is discussed below. Since the indenter tip generates a stress field nearby, the vertical component of the stress compresses the material downward, while the horizontal component pushes the material aside to form pile-ups if the top layer is ductile. Due to the different stress-strain responses of the materials in the multilayer structure, the applied stress could result in tension at the interface. Delamination occurs when the tension exceeds the adhesion strength. During loading, the multilayer structure (Cu, Ta, SiO_2 layer and Si substrate) is deformed. They were stretched down to conform to the shape of the tip. The upper layer might be even deformed more due to the larger stress. After unloading, the deformed layer tried to recover to some extent. The top Cu and Ta layer were deformed severely beyond the elastic recovery limit. Therefore, the stretched layers were unable to recover. The elongated layers were propped up by the partially recovered layers underneath, thus, they have a convex curve. The cumulative effect of multiple loadings, which doubled in each loading/unloading circle, could also enlarge the delamination. From the analysis above, when impacted by a large load and deformed, the Cu/Ta layers tend to delaminate from the SiO_2/Si layers in the Cu/Ti/SiO_2/Si multilayer structure. Thus, the Cu/Ta loses support from below in the concentrated stress deformation area. Therefore, these factors could exert negative effects on elec-

tromigration or the stress-induced migration properties of Cu at these deformed areas.

4. Conclusion

Cu/Ta/SiO_2/Si structured multilayers were prepared by magnetron sputtering on a thermal oxidized Si substrate with various thicknesses of Cu top layers. The stiff substrate exerts a distinct effect on the compound hardness and the elastic modulus, and dominates the mechanical properties under large loads. Delamination was found at the Ta/SiO_2 interface, which was attributed to different deformation behaviors of Cu layer, Ta layer, SiO_2 layer and Si substrate. Metal layers tend to be pushed outward, and are difficult to recover elastically. The brittle SiO_2 layer and Si substrate tend to release the loading energy by crack or fracture. Such differences in mechanical property, along with the cumulative effect of multiple-loading, contribute to the occurrence of delamination.

Acknowledgement

The authors are particularly grateful to Shanghai Hua Hong NEC Electronics Co., Ltd. for the TEM sample preparation and characterization.

References

[1] Torres J. Advanced copper interconnections for silicon CMOS technologies. Appl Surf Sci, 1995, 91: 112
[2] Torres J, Mermet J L, Madar R, et al. Copper-based metallization for ULSI circuits. Microelectron Eng, 1996, 34(1): 119
[3] Edelstein D, Heidenreich J, Goldblatt R, et al. Full copper writing in a sub-0.25 μm CMOS ULSI technology. IEEE IEDM, 1997, 97: 773
[4] Takasaga H, Adachi K, Takada M. A copper/polyimide metal-base packaging technology. J Electron Mater, 1989, 18(2): 319
[5] Lloyd J R, Clement J J. Electromigration in copper conductors. Thin Solid Films, 1995, 262: 135
[6] Ogawa E T, Lee K, Blaschke V A, et al. Electromigration reliability issues in dual-damascene Cu interconnections. IEEE Trans Reliab, 2002, 51(4): 403
[7] Li B, Sullivan T D, Lee T C, et al. Reliability challenges for copper interconnects. Microelectron Reliab, 2004, 44(3): 365
[8] Alam S M, Gan C L, Wei F L, et al. Electromigration reliability comparison of Cu and Al interconnects. IEEE Trans Device Mater Reliab, 2005, 5: 303
[9] Jackson R L, Broadbent E, Cacouris T, et al. Processing and integration of copper interconnects. Solid-State Technol, 1998, 41(3): 49
[10] Rosenberg R, Edelstein D C, Hu C K, et al. Copper metallization for high performance silicon technology. Annu Rev Mater Sci, 2000, 30: 229
[11] Latt K, Lee Y, Osipowicz T, et al. Interfacial reactions and failure mechanism of Cu/Ta/SiO_2 multilayer structure in thermal annealing. Mater Sci Eng B, 2002, 94(1): 111
[12] Stavreva Z, Zeidler D, Plötner M, et al. Characterization of Cu chemical mechanical polishing by electrochemical investigations. Microelectron Eng, 1997, 33: 249
[13] Wijekoon K, Mishra S, Tsai S, et al. Development of a production worthy copper CMP process. IEEE/SEMI Advanced Semiconductor Manufacturing Conference and Workshop, 1998: 354
[14] Steinlesberger G, Engelhardt M, Schindler G, et al. Processing technology for the investigation sub-50 nm copper damascene interconnects. Solid-State Electron, 2003, 47(7): 1237
[15] Fujiwara K, Tanimoto H, Mizubayashi H. Elasticity study of very thin Cu films. Mater Sci Eng A, 2006, 442: 336
[16] Lim B K, Park H S, Chin L K, et al. Bias-temperature stress analysis of Cu/ultrathin Ta/SiO_2/Si interconnect structure. J Vac Sci Technol B, 2004, 22: 2286
[17] Lee H J, Kwon K W, Ryu C, et al. Thermal stability of a Cu/Ta multilayer: an intriguing interfacial reaction. Acta Mater, 1999, 47: 3965
[18] Yuan Z L, Zhang D H, Li C Y, et al. Thermal stability of Cu/α-Ta/SiO_2/Si structure. Thin Solid Films, 2004, 462–463: 284
[19] Available online at HTTP://www.itrs.net
[20] Bhushan B. Nanotribology and nanomechanics. Wear, 2005, 259: 1507
[21] Oliver W, Pharr G. An improved technique for determining hardness and elastic modulus using load and displacement sensing indentation experiments. J Mater Res, 1992, 7(6): 1562
[22] Bhushan B, Koinkar V. Microtribological studies of doped single-crystal silicon and polysilicon films for MEMS devices. Sensors Actuators A, 1996, 57(2): 91
[23] Beck U, Smith D T, Reiners G, et al. Mechanical properties of SiO_2 and Si_3N_4 coatings: a BAM/NIST co-operative project. Thin Solid Films, 1998, 332: 164
[24] Beegan D, Chowdhury S, Laugier M. A nanoindentation study of copper films on oxidised silicon substrates. Surf Coat Tech, 2003, 176(1): 124
[25] Beegan D, Chowdhury S, Laugier M. The nanoindentation behaviour of hard and soft films on silicon substrates. Thin Solid Films, 2004, 466: 167
[26] Beegan D, Chowdhury S, Laugier M. Work of indentation methods for determining copper film hardness. Surf Coat Tech, 2005, 192(1): 57
[27] Beegan D, Chowdhury S, Laugier M. Comparison between nanoindentation and scratch test hardness (scratch hardness) values of copper thin films on oxidised silicon substrates. Surf Coat Tech, 2007, 201(12): 5804
[28] Zeng F, Gao Y, Li L, et al. Elastic modulus and hardness of Cu–Ta amorphous films. J Alloy Compd, 2005, 389(1): 75
[29] Saha R, Barnard J. Effect of structure on the mechanical properties of Ta and Ta(N) thin films prepared by reactive DC magnetron sputtering. J Cryst Growth, 1997, 174: 495
[30] Sneddon I. The relation between load and penetration in the axisymmetric boussinesq problem for a punch of arbitrary profile. Int J Eng Sci, 1965, 3(1): 47
[31] Randall N X, Holländer E, Julia-Schmutz C. Characterization of integrated circuit aluminum bonding pads by nanoindentation and scanning force microscopy. Surf Coat Tech, 1998, 99: 111
[32] Soare S, Bull S J, O'Neil A G, et al. Nanoindentation assessment of aluminum metallization; the effect of creep and pile-up. Surf Coat Tech, 2004, 177/178: 497